A correlation of the hydrogen evolution reaction activity to the number of defects formed by the decomposition of doped phosphorus species in carbon nanotubes

AI Jie, LIU Zi-wu*, SUN Mao-mao, LIU Ling, WANG Quan-de*

（*Jiangsu Key Laboratory of Coal-based Greenhouse Gas Control and Utilization*, *Jiangsu Province*, *School of Chemical Engineering and Jiangsu Province Engineering Laboratory of High Efficient Energy Storage Technology and Equipments*, *China University of Mining and Technology*, *Xuzhou* 221008, *China*）

Abstract: Phosphorus-doped carbon materials are one of the novel carbon catalysts for the hydrogen evolution reaction (HER) that have attracted considerable attention in recent years. However, the role of C—P species played in the HER activity is still not clear. Phosphorus-doped carbon nanotubes were prepared by chemical vapor deposition and annealed at 900, 1 000 and 1 200 °C to remove all or part of the phosporus, resulting in four samples with different amounts of substitutional-, pyridine- and pyrrole-like P species. The correlations between the HER activity and the contents of the three species were investigated. Results showed that the content of substitutional P decreased with annealing temperature and none was retained at 1 200 °C. The HER activity increased with annealing temperature and the sample annealed at 1 200 °C had the highest HER activity in an acid medium with an overpotential of 0.266 V at a current density of 10 mA cm^{-2}. Density functional theory calculations showed that the pentagon- and nine-membered ring defects formed by the elimination of substitutional P mainly contributed to the HER activity.

Key words: Phosphorus-doped carbon nanotube; C—P species; Defect; Hydrogen evolution reaction; Water splitting

1 Introduction

Since the doping of phosphorus into carbon skeleton was proved to be able to boost the electrocatalytic activity of carbon materials towards the oxygen reduction reaction[1–3], various phosphorus-doped carbon materials with different morphological characters were developed and displayed remarkable performances in ion batteries[4–6], supercapacitors[7–9] and water splitting[10–13]. However, for these emerging striking phosphorus-doped carbon materials, up to now, their active P species are still ambiguous mainly due to the coexistence of many different P species such as graphite-like P (C_3—P), pyridine- and pyrrole-like P (C_2—P), C_3—P=O, C—O—P= $O(OH)_2$, C—P= $O(OH)_2$, which impede their further practical application greatly. Our previous work[13] demonstrated that the defects resulted from the decomposition of C_3—P=O group and the C—O—P species contributed mainly to the performance improvement of hydrogen evolution reaction (HER) and oxygen evolution reaction (OER). The absence of C—P species such as C_2—P and C_3—P from the reported phosphorus-doped materials made their effects on HER performance unknown.

We prepared four phosphorus-doped carbon nanotubes (P-CNTs) with different P species to investigate the effects of graphite-, pyridine- and pyrrole-like three P species on the HER activity of phosphorus-doped carbon materials. Results indicated that the phosphorus-doped carbon nanotubes prepared at 1 200 °C with an overpotential of 0.266 V at the current density of 10 mA cm^{-2} exhibited a much high HER activity in an acid medium. Density functional theory (DFT) calculations further revealed that compared with the defects from the pyrolysis of pyridine- and pyrrole-like P species, the pentagon- and nine-member ring defects resulted from the decomposition of graphite-P species were the main active sites for the HER, providing a new perspective for the rational development of high-efficiency HER catalysts.

Received date: 2020-09-11; **Revised date:** 2020-11-27

Corresponding author: LIU Zi-wu. E-mail: lzwmsy@cumt.edu.cn;
WANG Quan-de. E-mail: 306088995@qq.com

Supplementary data associated with this article can be found in the online version.

2 Experimental

P-CNTs were synthesized by chemical vapor deposition with triphenylphosphine (TPP) as a phosphorus source, toluene as a carbon source, ferrocene and Fe-Mo/Al_2O_3 as catalysts. In a typical procedure, TPP, toluene and ferrocene were mixed at a mass ratio of 15∶100∶7.5. The tubular furnace was heated to 750 °C after a clean quartz boat with 0.1 g of Fe-Mo/Al_2O_3 catalysts was put into the high temperature area of the quartz tube[2]. The product in the quartz boat was collected and denoted as P-CNTs1. Finally, P-CNTs1 was calcined at 900, 1 000 and 1 200 °C under vacuum for 2 h to produce samples named as P-CNTs2, P-CNTs3 and P-CNTs4, respectively.

3 Results and discussion

The SEM and TEM images (Fig. 1) of P-CNTs1, P-CNTs2, P-CNTs3 and P-CNTs4 indicated that all of the four samples had a nanotube morphology. From the HRTEM images, it could be found that the carbon lattice fringes in P-CNTs1 were much more regular than those in P-CNTs4, indicating the presence of more edge defects in P-CNTs4.

The two dominant diffraction peaks near 23° and 43° in the XRD spectra of 4 samples (Fig. S1a) could be attributed to the (002) and (100) crystal planes of graphitic carbon, respectively, confirming that the prepared samples were mainly composed of CNTs. Raman spectra of four samples in Fig. 2 could be deconvoluted into *D*, *G*, *I* and *D*" peaks. The *D* and *G* bands at ca. 1 350 and 1 580 cm^{-1} reflect the degree of lattice defects and the E_{2g} vibration of carbon atoms, respectively. *I* band at ca.1 220 cm^{-1} corresponds to the disorder in the graphitic lattice, such as sp^2-sp^3 bonds and polyenes, and *D*" band at ca. 1 500 cm^{-1} is generally related to the amorphous carbon[14–16]. The I_D/I_G values of four samples increased from 0.47 to 1.78 as the synthesis temperature increased (Fig. 2), indicating that the defect degree of the materials increased

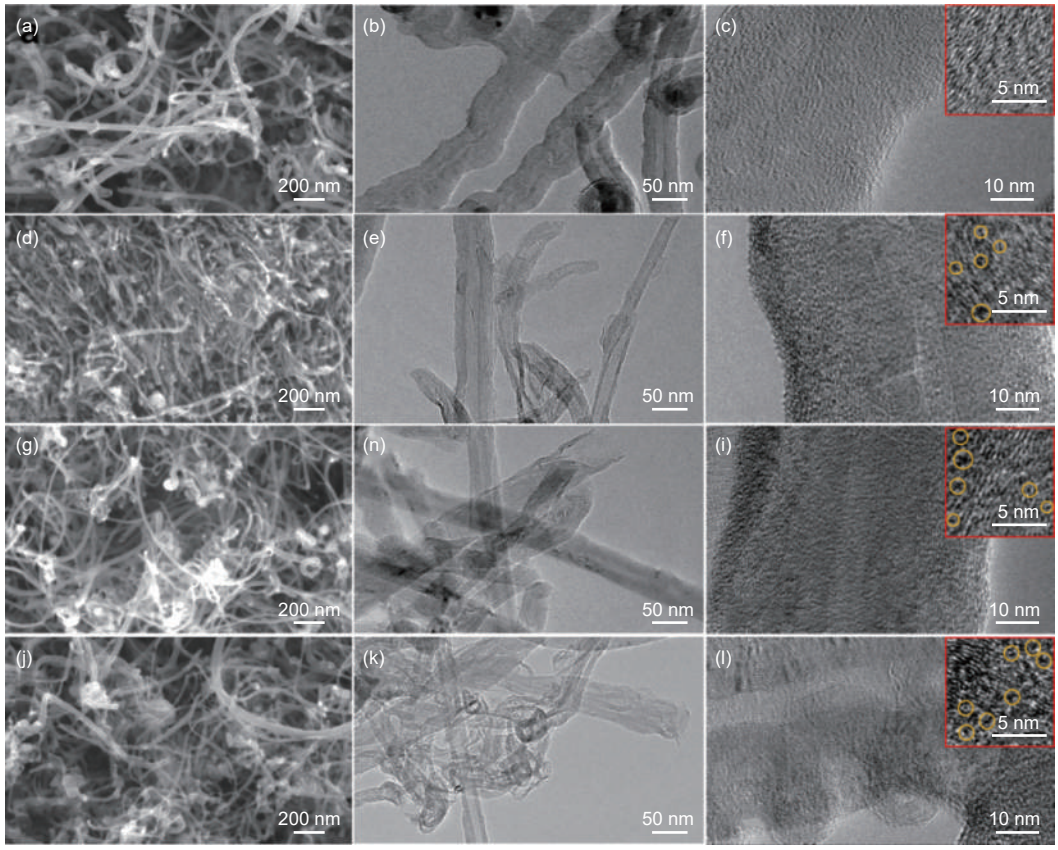

Fig. 1 SEM images of (a) P-CNTs1, (d) P-CNTs2 , (g) P-CNTs3 and (j) P-CNTs4 . TEM images of (b, c) P-CNTs1 , (e, f) P-CNTs2, (h, i) P-CNTs3 and (k, l) P-CNTs4 , and their HRTEM images inserted in their corresponding TEM images (c, f, i and l).

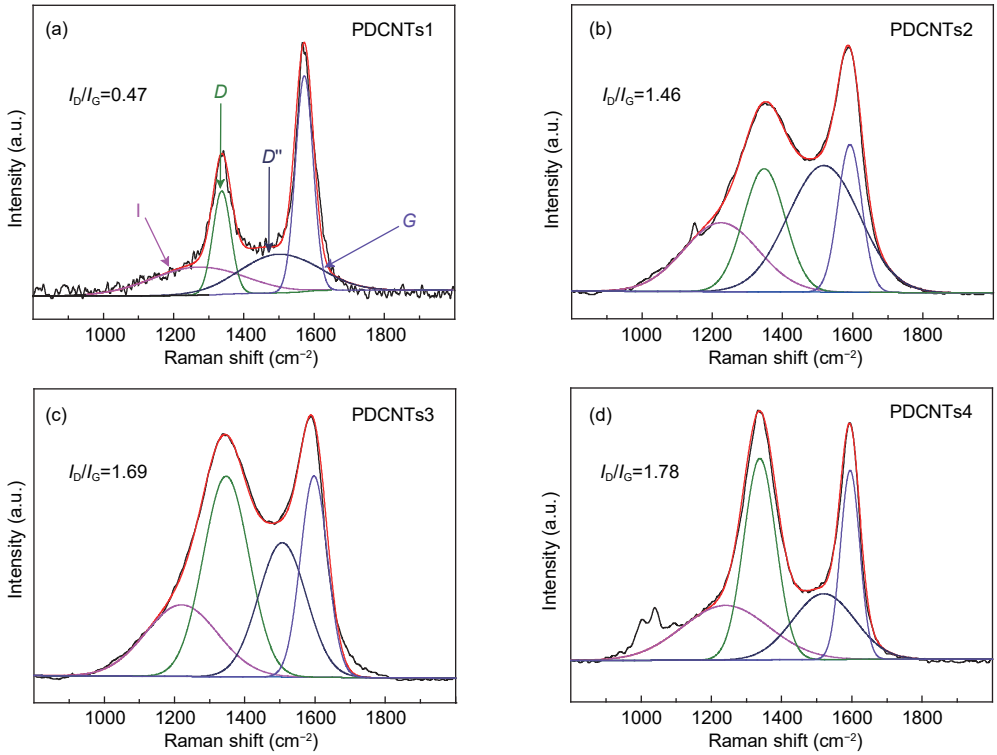

Fig. 2　Deconvoluted Raman spectra and I_D/I_G values of (a) P-CNTs1 , (b) P-CNTs2 , (c) P-CNTs3 and (d) P-CNTs4 .

with the synthesized temperature increase.

The XPS spectra in Fig. S1b show that P-CNTs1, P-CNTs2 and P-CNTs3 were mainly composed of C, O and P, and the P-CNTs4 only had C and O elements (Table 1). The four peaks at 284.8, 285.9, 286.9, and 289.5 eV deconvoluted from C 1s spectra (Fig. 3) could be attributed to sp^2, sp^3, C—O and π-π*, respectively[17]. The sp^3/sp^2 carbon ratios increased with the synthesis temperature (Table 2) . Meanwhile, four peaks at 130.6, 132.3, 133.1 and 134 eV in P2p spectra (Fig. 4) could be ascribed to C—P, C_3—P=O, C—P—O and C—O—P, respectively[18].

Fig. 5a and 5b show the HER electrocatalytic activities of four samples in an acidic medium, which indicated a gradual increase of their HER activities with the synthesis temperature. The P-CNTs4 as a HER catalyst had an overpotential of 0.266 V at a current density of 10 mA cm^{-2}, which was the best among them and superior to most of reported carbon-based metal-free electrocatalysts[13]. Fig. 5c indicated that the tafel slope (89.1 mV dec^{-1}) of P-CNTs4 was the smallest, suggesting the fastest HER kinetics of P-CNTs4 among the four samples. Meanwhile, Fig. 5d showed that the HER activities of four samples decreased with the increase of the C—P content, suggesting that C—P species could not promote HER directly. Interestingly, their HER activities increased with the increase of I_D/I_G values, implying that the breaking of C—P bonds in them would yield defects that improved the HER activity (Fig. 5d, Fig. S2). The Nyquist diagrams in Fig. 5e show that the P-CNTs4 had the smallest semicircle diameter, the least charge transfer resistance and the fastest catalytic kinetics. Meanwhile, Fig. 6 and 7 indicated that the HER activity of the four samples had a positive correlation with their electrochemically active surface area (ECSA). And the P-CNTs4 with the best HER activity exhibited an excellent stability as well (Fig. 5f), showing a good application prospect in future water electrolysis.

Table 1　Elemental contents in 4 samples from the XPS.

Samples	C	O	P			
			C—P	C_3—P=O	C—O—P	C—P—O
P-CNTs1	93.12%	6.52%	0.191%	0.109%	0.032%	0.028%
P-CNTs2	97.52%	2.20%	0.131%	0.082%	0.067%	0
P-CNTs3	97.98%	1.79%	0.119%	0.039%	0.072%	0
P-CNTs4	98.27%	1.73%	0	0	0	0

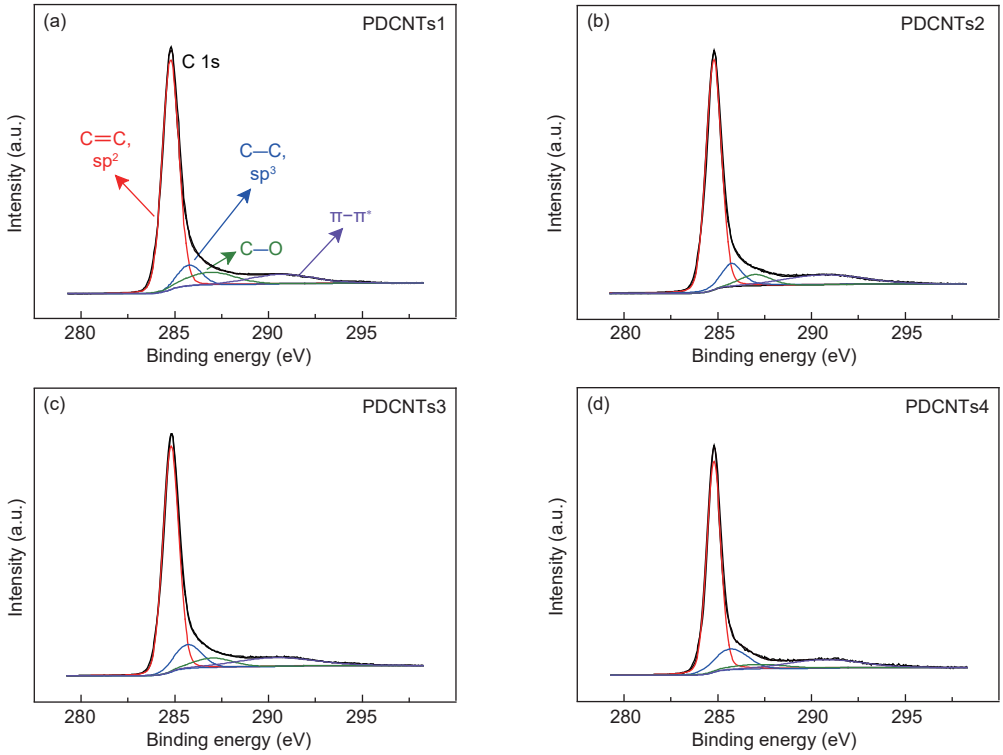

Fig. 3 The high-resolution C 1s spectra of (a) P-CNTs1, (b) P-CNTs2 , (c) P-CNTs3 and (d) P-CNTs4 .

Table 2 The contents of sp^2 and sp^3 carbons, C=O, C—O, π-π* and the ratios of sp^2/sp^3 carbon from the C 1s spectra.

Samples	sp^2	sp^3	sp^3/sp^2	C—O	π-π*
P-CNTs1	69.74%	8.77%	12.58	10.80%	10.69%
P-CNTs2	66.82%	10.84%	16.22	6.14%	13.73%
P-CNTs3	66.76%	11.66%	17.46	6.58%	12.98%
P-CNTs4	66.07%	14.40%	21.79	5.08%	12.71%

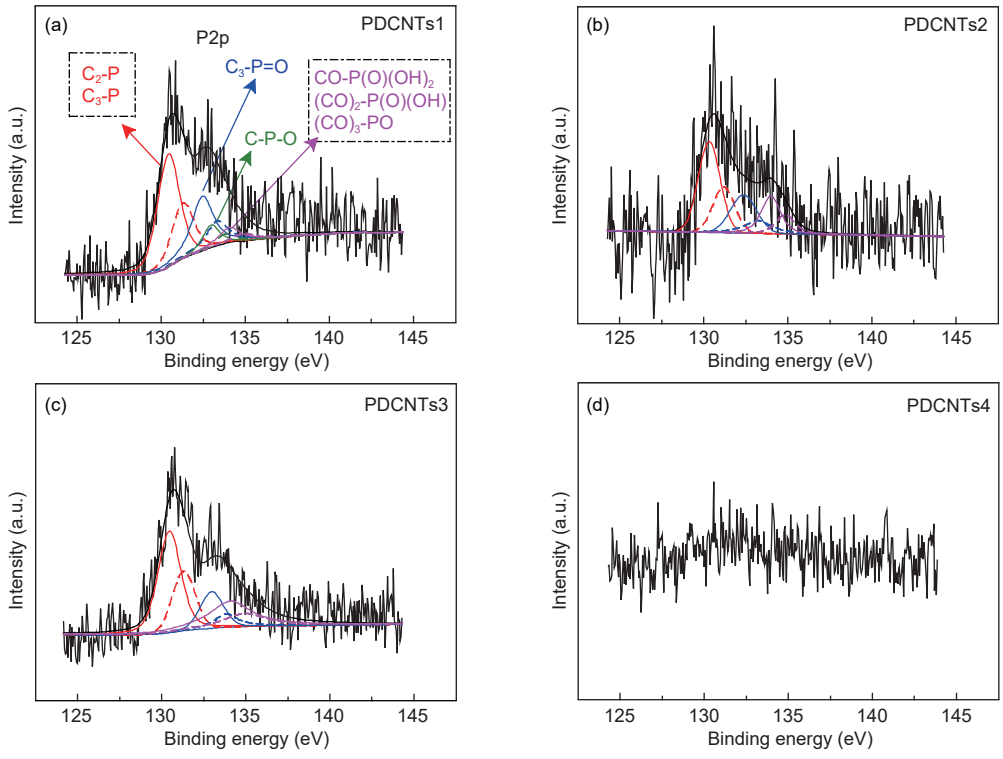

Fig. 4 The high-resolution P2p spectra of (a) P-CNTs1, (b) P-CNTs2 , (c) P-CNTs3 and (d) P-CNTs4 .

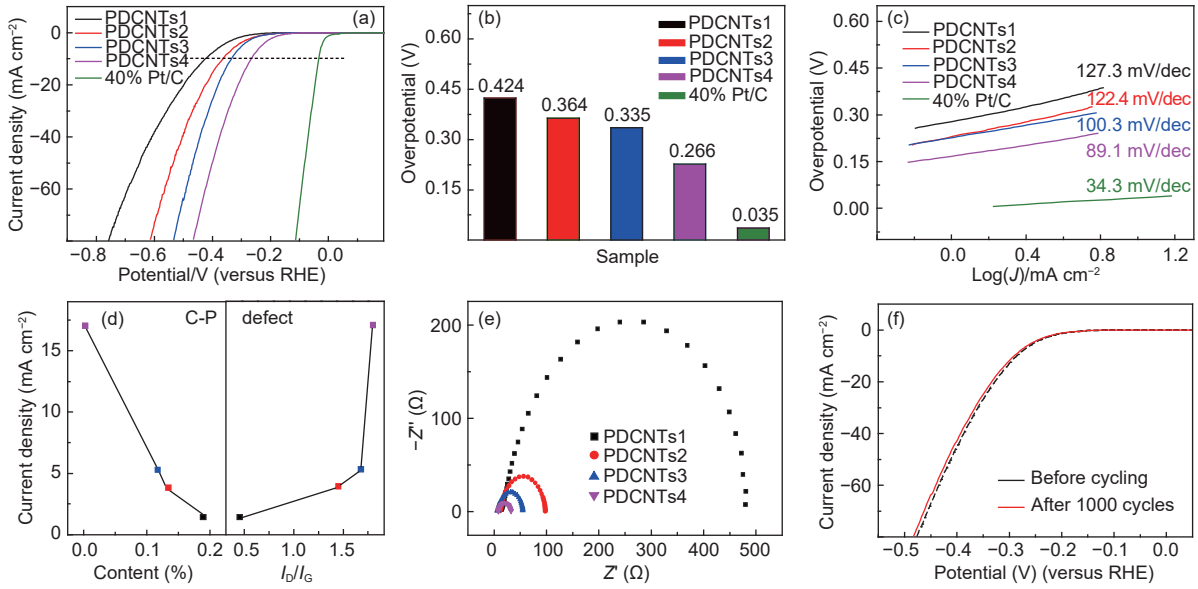

Fig. 5　(a) The HER polarization curves of P-CNTs1, P-CNTs2, P-CNTs3, P-CNTs4 and 40 wt% Pt/C catalysts in a N_2-saturated 0.5 mol L^{-1} H_2SO_4 solution, (b) Their corresponding overpotentials at the current density of 10 mA cm^{-2} and (c) tafel plots from (a), (d) The dependence of the HER current densities (at 300 mV overpotential) of P-CNTs1 (■), P-CNTs2 (■), P-CNTs3 (■), P-CNTs4 (■) on the C-P content and the values of I_D/I_G, (e) Impedance diagrams of P-CNTs1, P-CNTs2, P-CNTs3, and P-CNTs4, (f) The HER curves of P-CNTs4 in a 0.5 mol L^{-1} H_2SO_4 medium before and after 1 000 cycles.

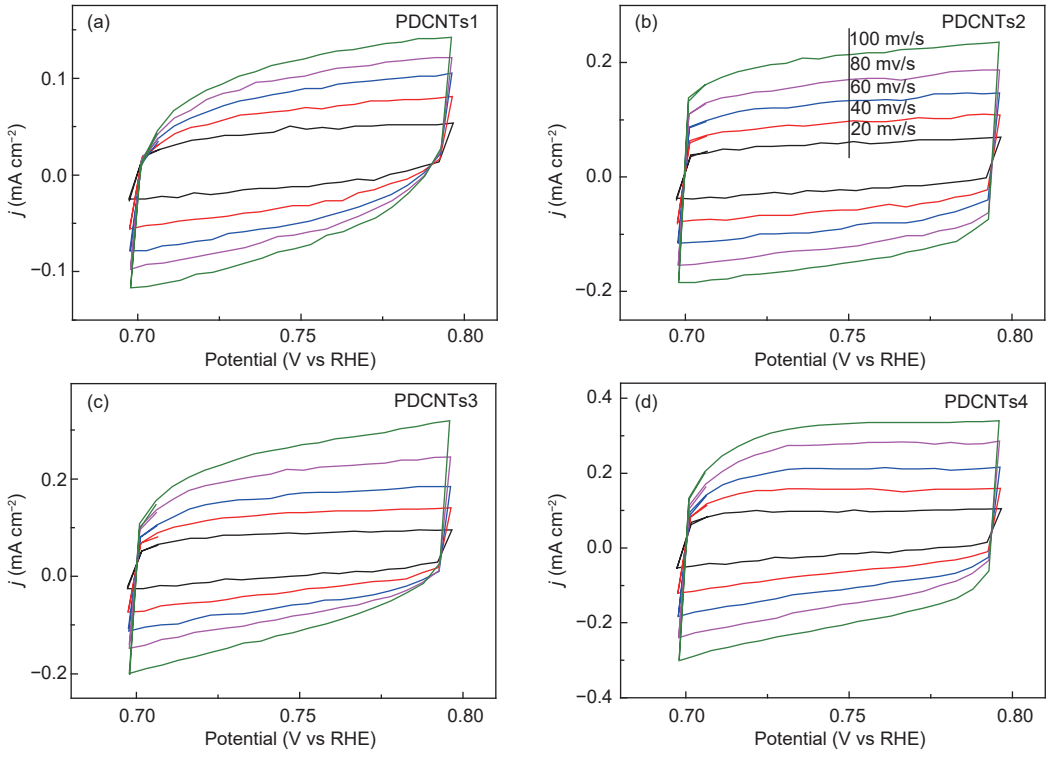

Fig. 6　Cyclic voltammograms of (a) P-CNTs1, (b) P-CNTs2, (c) P-CNTs3 and (d) P-CNTLs4 in 0.5 mol L^{-1} H_2SO_4 at different scan rates.

Since the breaking of C—P bonds would yield defects and bring about the improvement of the HER activity, as confirmed by turnover frequency (TOF) values at 0.3 V overpotential and the decrease of C—P contents (Table S3), we employed DFT to calculate the charge and spin densities of carbon atoms around graphite-P, pyridine-P and pyrrole-P to further ascertain what defects would form and which carbon

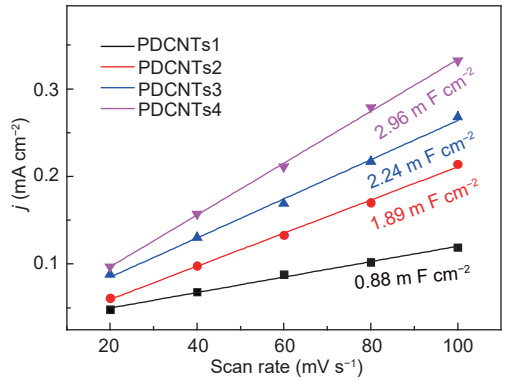

Fig. 7 The capacitive currents as a function of the scan rate for P-CNTs1, P-CNTs2, P-CNTs3 and P-CNTs4.

atoms would serve as HER active sites. Interestingly, results in Fig. 8 and Fig. 9 showed that with the breaking of C—P bonds in graphite-P in the CNT network, pentagon- and nine-membered rings defects would form. And the decomposition of pyridine-P and pyrrole-P would form armchair and pentagon zigzag defects (Fig. S3 and S4). Table 3, Table S1 and S2 indicated that the breaking of graphite-P bond would bring more changes in charge and spin densities of carbon atoms in pentagon- and nine-membered ring defects as compared with that of pyridine-P and

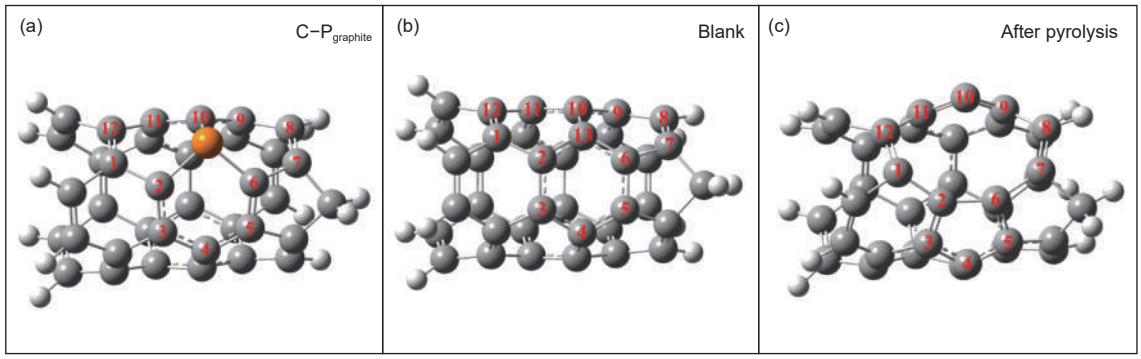

Fig. 8 (a) The CNTs with a C_3-P graphite-like configuration, (b) The blank normal CNT framework and (c) the CNTs with the pentagon- and nine-membered ring defects formed by the decomposition of C_3-P group.

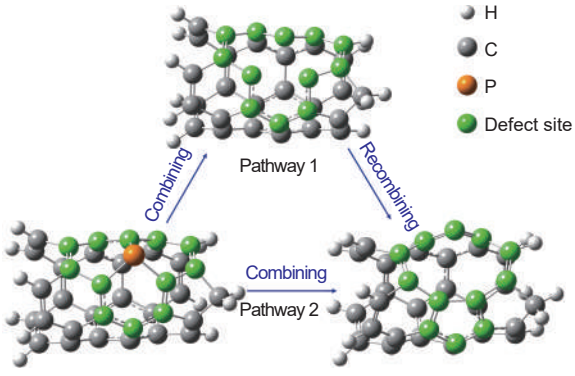

Fig. 9 The possible formation mechanism of pentagon- and nine-membered ring defects with the decomposition of the C_3-P group.

pyrrole-P, revealing that these two defects were mainly the HER active sites. To further explore active carbon atoms in pentagon- and nine-membered ring defects, the H^+ adsorption energy was also calculated by the DFT. Table 4 demonstrated that the H^+ adsorption energies on C3, C4 and C5 in the pentagon defect and those on C1, C9, C10 and C11 in the nine-membered ring defect were obviously larger than those of carbon atoms in the blank CNT network, implying that these seven carbon atoms in the two defects were the main HER active sites. Based on this finding, the possible HER routes were proposed in Fig. 10.

Table 3 The charge and spin densities (a.u.) of carbon atoms in the new formed defects after the decomposition of the C_3—P graphite-like structure and those of the corresponding carbon atoms in the blank.

Carbon atom	Charge density (Blank)	Spin density (Blank)	Charge density (After pyrolysis)	Spin density (After pyrolysis)
1	−0.009	0	−0.026	0
2	0	0	0.038	0
3	0	0	−0.067	0
4	0.018	0	−0.009	0
5	−0.014	0	−0.063	0
6	−0.014	0	0.034	0
7	0.035	0	0.030	0
8	−0.153	0	−0.143	0
9	0.016	0	−0.042	0
10	0.002	0	−0.073	0
11	0.002	0	−0.046	0
12	−0.021	0	0.009	0
13	0.019	0	–	–

Table 4　The H^+ adsorption energies (kcal mol^{-1}) on carbon atoms in the new formed defects from the decomposition of the C_3—P graphite-like structure and those of corresponding carbon atoms in the blank.

Carbon atom	Adsorption energies (kcal mol^{-1})	
	Pure CNT (blank)	CNT (after pyrolysis)
1	−58.163	−74.825
3	−56.805	−101.009
4	−55.909	−113.664
5	−58.719	−101.588
9	−55.458	−80.907
10	−55.824	−142.826
11	−57.595	−75.465

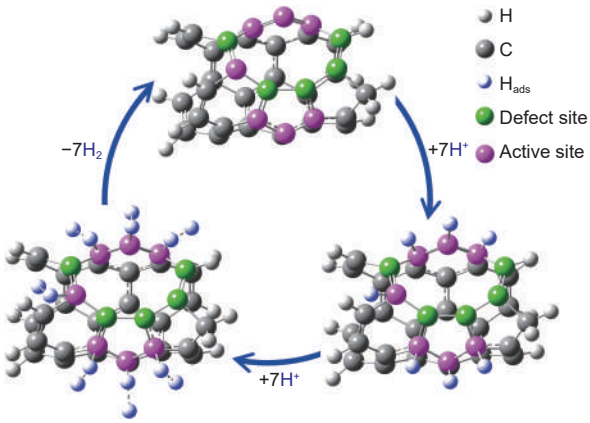

Fig. 10　The possible HER routes on P-CNTs in an acidic medium.

4　Conclusions

We have systematically explored the influence of C—P species on the HER performance of P-CNTs through the experimental investigation and theoretical calculation. Results indicated that the P-CNT4 had an overpotential of 0.266 V at the current density of 10 mA cm^{-2}, which exhibited a much high HER activity in an acid medium, and the decomposition of graphite-P species would form defects that boosted the HER of P-CNTs. DFT calculation further revealed that about seven carbon atoms in the pentagon- and nine-membered ring defects were mainly the HER active sites. This work provides a deep insight into the relationship between the type of P species and the HER performance.

Acknowledgement

This work was supported by Jiangsu Key Laboratory of Coal-based Greenhouse Gas Control and Utilization (2020ZDZZ04A, 2019B002).

References

[1] Liu Z W, Peng F, Wang H J, et al. Phosphorus-doped graphite layers with high electrocatalytic activity for the O_2 reduction in an alkaline medium[J]. Angew Chem Int Ed, 2011, 50: 3257-3261.

[2] Liu Z W, Peng F, Wang H J, et al. Novel phosphorus-doped multiwalled nanotubes with high electrocatalytic activity for O_2 reduction in alkaline medium[J]. Catal Commun, 2011, 16: 35-38.

[3] Liu Z W, Peng F, Wang H J, et al. Preparation of phosphorus-doped carbon nanospheres and their electrocatalytic performance for O_2 reduction[J]. J Nat Gas Chem, 2012, 21: 257-264.

[4] Hou H S, Shao L D, Zhang Y, et al. Large-area carbon nanosheets doped with phosphorus: A high-performance anode material for sodium-ion batteries[J]. Adv Sci, 2017, 4: 1600243.

[5] Li K, Hu Z Y, Ma J Z, et al. A 3D and stable lithium anode for high-performance lithium-iodine batteries[J]. Adv Mater, 2019, 31: 1902399.

[6] Wang J X, Xia Y, Liu Y, et al. Mass production of large-pore phosphorus-doped mesoporous carbon for fast-rechargeable lithium-ion batteries[J]. Energy Storage Materials, 2019, 22: 147-153.

[7] Wen Y Y, Wang B, Huang C C, et al. Synthesis of phosphorus-doped graphene and its wide potential window in aqueous supercapacitors[J]. Chem Eur J, 2014, 20: 1-7.

[8] Yang W, Yang W, Kong L N, et al. Phosphorus-doped 3D hierarchical porous carbon for high-performance supercapacitors: A balanced strategy for pore structure and chemical composition[J]. Carbon, 2018, 127: 557-567.

[9] Lv B J, Li P P, Liu Y, et al. Nitrogen and phosphorus co-doped carbon hollow spheres derived from polypyrrole for high-performance supercapacitor electrodes[J]. Applied Surface Science, 2018, 437: 169-175.

[10] Zheng Y, Jiao Y, Li L H, et al. Toward design of synergistically active carbon-based catalysts for electrocatalytic hydrogen evolution[J]. ACS Nano, 2014, 8: 5290-5296.

[11] Xiao Z H, Huang X B, Xu L, et al. Edge-selectively phosphorus-doped few-layer graphene as an efficient metal-free electrocatalyst for the oxygen evolution reaction[J]. Chen Commun, 2016, 52: 13008-13011.

[12] Jiang H L, Zhu Y H, Su Y H, et al. Highly dual-doped multilayer nanoporous graphene: efficient metal-free electrocatalysts for the hydrogen evolution reaction[J]. J Mater Chem A, 2015, 3: 12642-12645.

[13] Liu Z W, Ai J, Sun M M, et al. Phosphorous-doped graphite layers with outstanding electrocatalytic activities for the oxygen and hydrogen evolution reactions in water electrolysis[J]. Adv Funct Mater, 2020, 30: 1910741.

[14] Mcevoy N, Peltekis N, Kumar S, et al. Synthesis and analysis of thin conducting pyrolytic carbon films[J]. Carbon, 2012, 50: 1216-1226.

[15] Zhou Y, Ma R G, Candelaria S L, et al. Phosphorus/sulfur Co-

doped porous carbon with enhanced specific capacitance for supercapacitor and improved catalytic activity for oxygen reduction reaction[J]. J Power Sources, 2016, 314: 39-48.

[16] Tian X D, Li X, Yang T, et al. Flexible carbon nanofiber mats with improved graphitic structure as scaffolds for efficient all-solid-state supercapacitor[J]. Electrochim Acta, 2017, 247: 1060-1071.

[17] Liu Z J, Zhao Z H, Wang Y Y, et al. In situ exfoliated, edge-rich, oxygen-functionalized graphene from carbon fibers for oxygen electrocatalysis[J]. Adv Mater, 2017, 29: 1606207.

[18] Bi Z H, Luo L, Kong Q Q, et al. Structural evolution of phosphorus species on graphene with a stabilized electrochemical interface[J]. ACS Appl Mater Interfaces, 2019, 11: 11421-11430.